Heliyon 10 (2024) e27803

Contents lists available at ScienceDirect

Heliyon

journal homepage: www.cell.com/heliyon

Research article

Single-nucleus RNA and multiomics in situ pairwise sequencing reveals cellular heterogeneity of the abnormal ligamentum teres in patients with developmental dysplasia of the hip

Zhenhui Zhao [a,b,1], Chuiqin Fan [a,b,1], Shiyou Wang [c,d,1], Haoyu Wang [c,d,1], Hansheng Deng [a], Shuaidan Zeng [a], Shengping Tang [a,***], Li Li [e,****], Zhu Xiong [a,b,**], Xin Qiu [a,*]

[a] Shenzhen Children's Hospital, Shenzhen, Guangdong Province, China
[b] China Medical University, Shenyang, Liaoning Province, China
[c] Key Laboratory of Synthetic Biology Regulatory Elements, Institute of Systems Medicine, Chinese Academy of Medical Sciences & Peking Union Medical College, Beijing, China
[d] Suzhou Institute of Systems Medicine, Suzhou, China
[e] Shenzhen Luohu Maternity and Child Healthcare Hospital, Shenzhen, Guangdong Province, China

ARTICLE INFO

Keywords:
Cellular heterogeneity
Developmental dysplasia of the hip
Ligamentum teres
Multiomics in situ pairwise sequencing
Single-nucleus RNA sequencing

ABSTRACT

Developmental dysplasia of the hip (DDH) is the most common hip deformity in pediatric orthopedics. One of the common pathological changes in DDH is the thickening and hypertrophy of the ligamentum teres. However, the underlying pathogenic mechanism responsible for these changes remains unclear. This study represents the first time that the heterogeneity of cell subsets in the abnormal ligamentum teres of patients with DDH has been resolved at the single-cell and spatial levels by snRNA-Seq and MiP-Seq. Through gene set enrichment and intercellular communication network analyses, we found that receptor-like cells and ligament stem cells may play an essential role in the pathological changes resulting in ligamentum teres thickening and hypertrophy. Eight ligand–receptor pairs related to the ECM–receptor pathway were observed to be closely associated with DDH. Further, using the Monocle R package, we predicted a differentiation trajectory of pericytes into two branches, leading to junctional ligament stem cells or fibroblasts. The expression of extracellular matrix-related genes along pseudotemporal trajectories was also investigated. Using MiP-Seq, we determined the expression distribution of marker genes specific to different cell types within the ligamentum teres, as well as differentially expressed DDH-associated genes at the spatial level.

* Corresponding authors.
** Corresponding author. Shenzhen Children's Hospital, Shenzhen, Guangdong Province, China.
*** Corresponding authors.
**** Corresponding author.
E-mail addresses: tangshengping56@126.com (S. Tang), 1748852622@qq.com (L. Li), bamboobear@163.com (Z. Xiong), qiuxinfrank@163.com (X. Qiu).
[1] These authors have contributed equally to this work.

https://doi.org/10.1016/j.heliyon.2024.e27803
Received 2 September 2023; Received in revised form 22 February 2024; Accepted 6 March 2024
Available online 15 March 2024

1. Introduction

Developmental dysplasia of the hip (DDH) is the most common congenital disorder of the musculoskeletal system in newborns [1]. Depending on the case definition and ethnicity, the reported prevalence of DDH at birth ranges from 1.9% to 30% of live births [2]. It is widely believed that DDH is caused by complex polygenic inheritance and environmental factors. 12%–33% of children with DDH have a positive family history [3]. Siblings of children with DDH have a 10-fold increased incidence [4]. Currently, through the implementation of genome-wide association studies, whole-exome sequencing, and other research methods, many candidate genes have been confirmed to be related to DDH, such as *CX3CR1*, *GDF5*, *ASPN*, and *COL1A1* [5]. In addition, there are many risk factors for DDH, such as joint laxity, swaddling position, breech presentation, oligohydramnios, and multiple pregnancies [6,7]. Nonetheless, the exact genetic model and pathogenesis of DDH remain unclear.

The treatment principles for DDH involve early diagnosis, gentle reduction, moderate hip flexion, and abduction to maintain precise concentric reductions [8,9]. However, complete concentric reductions of the femoral head are often hindered by soft tissue obstruction. An example of such pathology in DDH is thickened, hypertrophied ligamentum teres, which is known to impede femoral head reduction [10]. With regard to the pathogenesis of DDH, there are limited reports in the literature on the pathogenesis of the ligamentum teres. Current studies investigating the pathogenic mechanism of the ligamentum teres mainly focus on using histological staining to explore changes in its tissue structure at the molecular level [10,11]. However, considering the heterogeneity of individual cells, this approach has limitations in understanding tissue biology and resolving diverse disease states [12].With bulk RNA-Seq, although we can acquire average gene expression levels within a cell population, discerning disparities in gene expression among individual cells poses a challenge. Furthermore, it is notable that the results of bulk RNA-Seq fail to accurately reflect heterogeneity among cells. To overcome these challenges, single-cell RNA-Seq serves as a valuable tool. Single-cell RNA-Seq enables the identification of specific cell types, states, pathways, and the environment in which disease-related genes are involved, revealing the genetic structure and gene expression status of individual cells. Moreover, the results of single-cell RNA-Seq can effectively capture heterogeneity among cells [13].

In this study, we employed single-nucleus RNA sequencing (snRNA-Seq) and multiomics in situ pairwise sequencing (MiP-Seq) to analyze cellular heterogeneity of the abnormal ligamentum teres in patients with DDH. We aimed to investigate the underlying causes of ligamentum teres thickening and hypertrophy in these children at the single-cell and spatial levels. Our analyses revealed six cell types, among which receptor-like cells and ligament stem cells appeared to have a close association with DDH. Ligament stem cells play an essential role in the pathological changes leading to the thickening and hypertrophy of the ligamentum teres. Pseudotemporal analysis results indicated that pericytes may differentiate into fibroblasts and ligament stem cells. In addition, we constructed an intercellular communication network between different cell types within the ligamentum teres. By employing MiP-Seq, we determined the expression distribution of marker genes specific to different cell types within the ligamentum teres, as well as differentially expressed DDH-associated genes at the spatial level. To facilitate effective communication of our findings, results obtained on analyzing ligamentum teres single-cell sequencing data have been made available through the Musculoskeletal Cell Atlas (MSKCA, http://www.mskca.tech/Ligament/). This platform provides interactive visualizations, aiding users in efficiently exploring gene expression patterns and enhancing their understanding of our research findings. We believe that our data will serve as a valuable resource for constructing a cell atlas for human musculoskeletal diseases, as well as offer new ideas and methodologies for further exploring the pathogenesis of DDH.

2. Materials and methods

Ethical statement

This study was reviewed and approved by our hospital's ethics committee (Institution Review Board approval numbers: 202300202). Before conducting this study, the parents or legal guardians of the children were informed of the purpose of this study and signed an informed consent form.

2.1. Sample collection and nucleus extraction

According to the inclusion and exclusion criteria [14], abnormal ligamentum teres samples were collected from patients with DDH during open reduction surgery (Table S1). The inclusion criteria were as follows: (1) children diagnosed with DDH based on medical history, symptoms, signs, and related imaging examinations and (2) children with DDH who underwent open reduction and ligamentum teres resection. The exclusion criteria were as follows: (1) neuromuscular hip dislocation; (2) pathological hip dislocation; (3) traumatic, suppurative hip arthritis and other secondary hip dislocations; and (4) collagen metabolism-related diseases and other congenital musculoskeletal disorders.

The collected ligamentum teres tissues were washed with 1 × PBS, snap-frozen in liquid nitrogen, and stored until nuclei extraction. All samples stored for less than six months. Nuclei were extracted using the mechanical extraction method. Add 2 mL of pre-chilled lysis buffer to Dounce Tissue Grinders. Take an appropriate amount of tissue (60∼100 mg) in a grinder (5 mL). Grind 5–10 times with a fine pestle and five times with a coarse pestle.Incubate on ice for 5 min.During incubation, the pipette tip can mix the tissue homogenate gently and slowly to make the reaction more complete. Filter the homogenate through a 75 μm cell sieve.Centrifuge at 500×*g* for 5 min at four °C, remove the supernatant liquid and do not touch the nuclear pellet. Add 2 mL of resuspension buffer, gradient centrifugation solution, and centrifuge to remove the supernatant. Add an appropriate amount of PBS (containing 0.5% BSA)

to resuspend the nuclei. PI staining and countstar were used to detect the number of nuclei. Adjust the concentration of cell nucleus suspension to 1000 nuclei/μL [15–17].

2.2. Hematoxylin–eosin (HE) staining

To begin with, tissue samples were dehydrated. After paraffin embedding, sections with a thickness of 3 μm were obtained, which were then baked in an oven at 60 °C for 30 min. Staining was performed by immersing the slices in xylene I for 10 min, xylene II for 5 min, and xylene III for 5 min. Subsequently, they were treated with absolute ethanol for 5 min, followed by immersion in absolute ethanol for 2 min, 95% alcohol for 2 min, and 80% alcohol for 2 min. The slices were washed with water for 2 min, and then stained with hematoxylin for 1–5 min, followed by a 5-min water wash. After treating with the differentiation solution, the slices were rinsed with warm water until they turned blue. Eosin staining was performed for 5 min, and the samples were then dehydrated with 80% ethanol for approximately 1–2 min, followed by 95% ethanol for approximately 2 min and absolute ethanol for approximately 4–8 min. The slices were made transparent by immersing them in xylene for 2 min; this step was repeated, as needed. Finally, the slides were sealed, dried, and observed under a microscope.

2.3. MASSON staining

For MASSON staining, the procedure involved routine dewaxing to hydration. The slices were stained with iron hematoxylin staining solution for 5–10 min, followed by a 1-min water wash. They are then returned to blue for 3–7 min and washed with water for 1 min. Next, the slices were stained with ponceau red fuchsin staining solution for 2–5 min. The weak acid working solution was applied for 1 min and then discarded. Phosphomolybdic acid solution was added for 1–3 min, followed by a 1-min application of the weak acid working solution without discarding it. Subsequently, the slices were stained with aniline blue staining solution for 1–4 min; the weak acid working solution was then applied for 1 min and later discarded. Finally, the slices were dehydrated, made transparent, sealed, dried, and observed under a microscope.

2.4. SnRNA-Seq library construction

cDNA amplification and library construction were performed following the protocol provided the DNBelab C Series Single-Cell Library Prep Kit (MGI, #1000021082). After library preparation, sequencing was conducted on the DNBSEQ-G400 (BGISEQ-500) sequencing platform.

2.5. Pre-processing and quality control of snRNA-Seq data

First, we processed the raw sequencing data of each sample using DNBelab C Series scRNA analysis software (v3.2). Subsequently, we obtained the gene expression matrix for each sample, which included three files: matrix.mtx.gz, features.tsv.gz, and barcodes.tsv.gz [15]. Second, we employed the Seurat R package (v4.0.3) to perform cellular quality control and cluster analysis on scRNA-Seq data [18]. Briefly, we loaded the matrix.mtx.gz file for each sample using the readMM function of the Seurat package, resulting in a sparse matrix of UMI counts. In addition, we used the read.table function to read the barcodes.tsv.gz and features.tsv.gz files of each sample, retrieving barcodes and features, respectively. The barcodes and features were then assigned to the column and row names of the sparse matrix, respectively. Simultaneously, we utilized the CreateSeuratObject function of the Seurat package to read the modified sparse matrix and create a Seurat object. For this object, we applied the following criteria to filter out low-quality cells and low-expressed genes: cells with a number of detected genes (nFeature_RNA) < 500 or >3000 were excluded. To minimize the influence of noise on cell clustering, we deleted ribosome- and mitochondria-related genes using the method reported by Xue et al. [19]. We then employed the NormalizeData function (normalization.method = "LogNormalize") of the Seurat package to correct cell depth and the FindVariableFeatures function (selection. method = "vst") to identify the top 2000 hypervariable genes.

Next, we identified the anchor points of all samples using the FindIntegrationAnchors function (reduction = "canonical correlation analysis"). Subsequently, we integrated all samples using the IntegrateData function to obtain the integrated Seurat object. To ensure data expression values approximated a normal distribution, we employed the ScaleData function. In addition, principal component analysis was performed using the top 2000 hypervariable genes. Next, we evaluated the contribution of the top 50 principal components (PCs) to overall variance using the JackStraw and ElbowPlot functions of the Seurat package. We chose the top 10 PCs with the most significant p-values for uniform manifold approximation and projection (UMAP) and cell clustering. The UMAP visualization allowed us to evaluate the distribution of cells from different samples and identify possible batch effects. Further, to determine an appropriate resolution for cell subpopulation identification, we estimated the specificity of cell subpopulation marker genes at various resolutions using the method reported by Chaffin et al. [20]. The FindAllMarks function (test.use = "ROC") of the Seurat package was utilized to evaluate the area under the curve (AUC) values of the cell subpopulation marker genes at different resolutions. We gradually increased the resolution from 0.05 to 1.0 in increments of 0.05, stopping once the AUC values of all marker genes in a cell subpopulation at a particular resolution were <0.70. Ultimately, we determined a resolution of 0.2 for cluster analyses.

2.6. Differential expression analysis, gene ontology (GO) enrichment analysis, and cell-type annotation

To compare gene expression between different clusters, we utilized the FindAllMarks function of the Seurat package (test.use =

"wilcox," logfc.threshold = 2). Genes exhibiting differential expression in different clusters with a corrected p-value ≤0.05 were considered significant. To perform overexpression enrichment analysis on these differentially expressed genes within each cluster, we employed the clusterProfiler R package (v4.4.4) [21]. In the process of cell-type annotation, we assigned cell types to different clusters based on differential gene expression patterns, known marker genes of cell types from published articles, and results of functional enrichment analysis. In addition, we downloaded single-cell data of mouse ligaments from Gene Expression Omnibus (GSE194427) and performed cell-type annotation as per the aforementioned analysis method [22].

2.7. Collection and enrichment analysis of metabolic gene sets

Collagen-related metabolic abnormalities in the ligamentum teres could lead to DDH development [10,23,24]. To investigate the potential metabolic functions of different cell types in the ligamentum teres, we collected a metabolism-related gene set (Table S2) from a study by Wu et al. [25] and performed gene set enrichment analysis. Besides, to comprehensively characterize the biological functions of different cell types beyond metabolism, we obtained the Kyoto Encyclopedia of Genes and Genomes (KEGG) gene set (Table S3) from the Molecular Signatures Database (MSigDB) [26,27] using the MSigDB R package (v7.5.1, http://www.gsea-msigdb.org/gsea/msigdb/). Further, we performed gene set enrichment analysis using different methods, including AUCell (v1.14.0) [28], UCell (v1.1.0) [29], SingScore (v1.12.0) [30], and ssGSEA (v1.40.1) [31], to account for sample background information bias. Next, differential gene sets in the enrichment score matrix were identified using the Wilcox test, with corrected p-value threshold of <0.05 (Bonferroni correction method). Finally, to comprehensively evaluate the enrichment results, we employed the robust rank aggregation algorithm from the RobustRankAggreg package (v1.1.0) [32]. Subsequently, we chose gene sets that showed significant enrichment ($p < 0.05$) across multiple analysis methods and visualized them as a heatmap.

2.8. Collection of DDH-associated genes

Many candidate genes have been confirmed to be related to DDH through candidate gene association studies, genome-wide association studies, whole-exome sequencing, and other research methods [33–36] (Table S4).However, the detailed mechanisms of these genes in terms of cell-specific mechanisms remain unclear. Therefore, we followed the research methods of Doolittle ML et al. [37]and Qiu X et al. [38] to explore the expression differences of these DDH-related genes in different cell types of the ligamentum teres. This will help us identify key cell types that express DDH-related genes. We visualized their expression in different cell types using bubble plots. Subsequently, we compared their expression levels in different cell types using the FindAllMarks function (test.use = "wilcox," logfc.threshold = 2). Finally, we identified DDH-associated genes that exhibited differential expression in different cell types with a corrected p-value of ≤0.05.

2.9. Protein–protein interaction (PPI) network construction

PPI networks represent the interaction relationship between proteins and provide insights into protein function, complex biological processes (BPs), and signal transmission networks. Moreover, they facilitate the identification of new protein targets and drugs. In a PPI network, each protein is represented as a node, and interactions between proteins are represented as edges [39]. In the context of ligament stem cells, we constructed a PPI network using STRING [40]. From this PPI network of differential genes in ligament stem cells, we identified significant central genes.

2.10. Trajectory analysis

Mesenchymal stromal cells, fibroblasts, and pericytes reportedly exhibit similarities in biological characteristics and cell surface markers [41]. To gain a better understanding of the differentiation relationship between ligament stem cells, fibroblasts, and pericytes, we assessed their relative degrees of differentiation using the CytoTRACE R package (v0.3.3) [42]. We constructed pseudotemporal differentiation trajectories using the Monocle R package (v2.24.1) [43]. CytoTRACE utilizes the number of genes expressed per cell as a marker of developmental potential and infers the relative degree of cell differentiation based on a single-cell count matrix. We defined less differentiated pericytes as the starting point of pseudotemporal differentiation trajectories. Monocle was used to construct quasi-chronological trajectories of ligament stem cells, fibroblasts, and pericytes. The construction process involved creating a monocle object using the newCellDataSet function (lowerDetectionLimit = 0.5), evaluating size factors using the estimateSizeFactors function, estimating data dispersion using the estimateDispersions function, filtering low-quality genes (each gene expressed in at least three cells) using the detectGenes function, and also filtering genes with mean expression levels of ≤0.1 (mean_expression >0.1) using the Subset function. To complete the construction of the quasi-chronological trajectory, we applied the setOrderingFilter, reduceDimension (reduction_method = "DDRTree," max_components = 2, norm_method = "log"), and orderCells functions. Based on the pseudotemporal trajectory, we observed the differentiation of pericytes into fibroblasts and ligament stem cells at node 1. We identified 656 differentiation-related genes using the BEAM function (q-value < 1e−4, p < 1e−4); visualization was achieved using the ComplexHeatmap R package (v2.15.1), with a focus on the expression of extracellular matrix (ECM)-related genes along the pseudo-chronological trajectory.

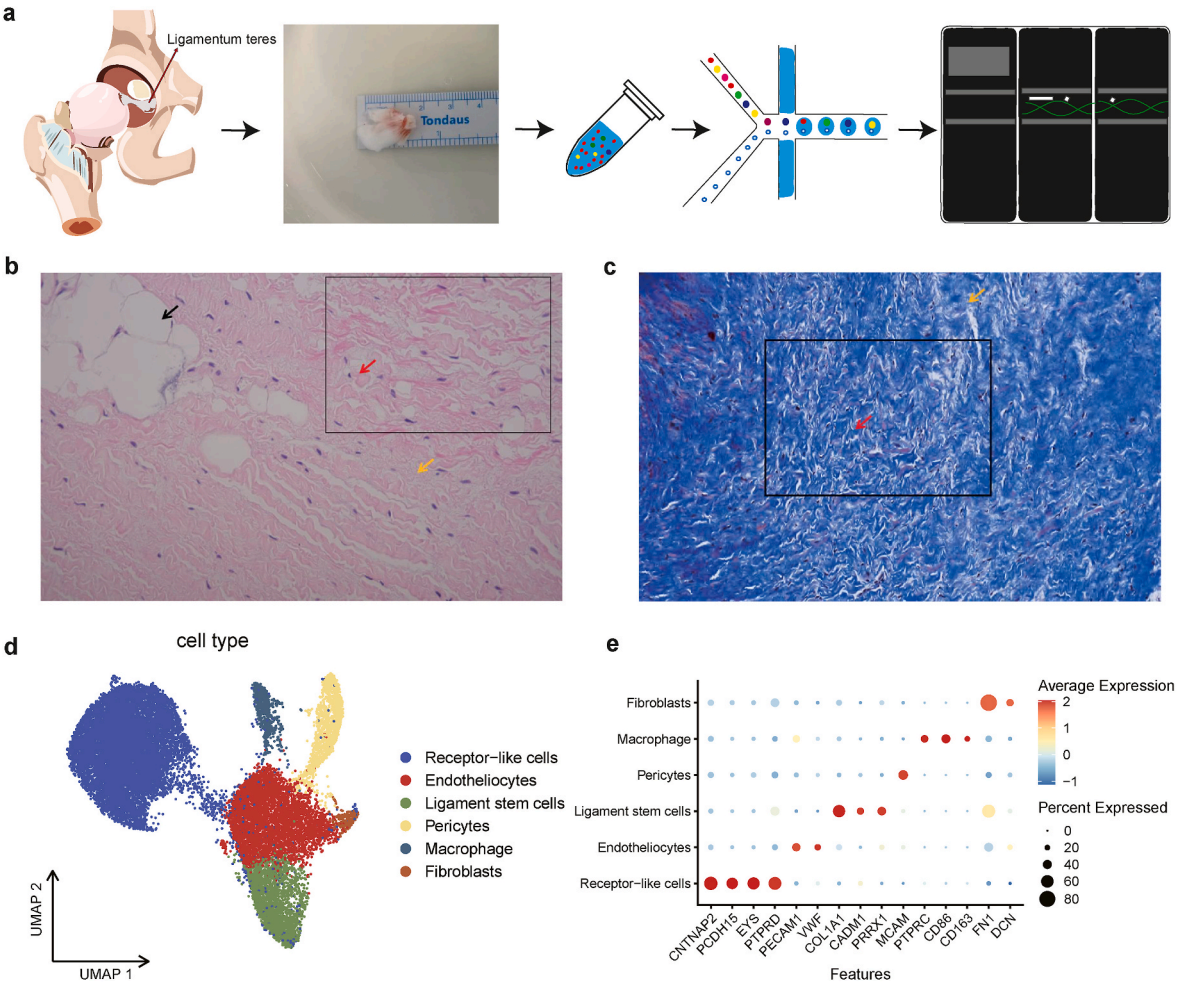

(caption on next page)

Fig. 1. The cell type annotation of the snRNA-Seq of ligamentum teres.
(a) Experimental flowchart illustrating the experimental design for snRNA-Seq of the ligamentum teres of children with DDH.
(b) HE staining of the ligamentum teres (× 40), showing fatty degeneration (black arrow), loose and disordered arrangement of fibrous connective tissue (black rectangular frame), decreased number of elastic fibers, visible breakage (red arrow), and increased collagen fibers (yellow arrow).
(c) MASSON staining (× 40), showing loose and disordered arrangement of fibrous connective tissue (black rectangular frame), decreased number of elastic fibers, breakage of elastic fibers (red arrow), and increased collagen fibers (yellow arrow).
(d) UMAP plot depicting the single-cell map of the ligamentum teres. Colors represent different cell types.
(e) Bubble plot showing the expression of marker genes used to annotate cell types. Circle color represents the average marker gene expression scale in different cell types, and circle size depicts marker gene expression ratio in different cell types.
(f) UMAP plot showing the expression of different marker genes in the ligamentum teres cell atlas. Brighter colors represent higher expression levels.
(For interpretation of the references to color in this figure legend, the reader is referred to the Web version of this article.)

2.11. Construction of an intercellular communication network

To gain insights into the intercellular communication among different cell subpopulations in the ligamentum teres, we employed the CellChat R package (v1.1.3) [44] to construct an intercellular communication network. The analysis process involved creating a CellChat object using the createCellChat function; for this purpose, the human ligand–receptor interaction database was used. Next, we identified overexpressed ligands or receptors and projected gene expression data onto a PPI network. We then assigned a probability value to each ligand–receptor interaction through permutation tests to identify statistically significant interactions. Each ligand–receptor interaction was assigned to a signaling pathway, and the communication probability for each signaling pathway was calculated by integrating the probabilities of all interactions associated with each signaling pathway, which were later summarized. We visualized statistically significant ligand–receptor pairs and their distribution across different cell types using bubble and chord plots.

2.12. MiP-Seq

Spatial FISH Ltd. designed specific probes for target RNA. Tissue samples were fixed, dehydrated, and embedded in paraffin, followed by sectioning into 3 μm slices using a paraffin microtome. These samples were then subjected to a series of reactions, including fixation in 4% paraformaldehyde, dehydration with methanol, denaturation, and hybridization with specific targeting probes in a reaction chamber at 37 °C for overnight. Subsequently, they were washed thrice with PBST, followed by ligation of target probes in ligation mix at 25 °C for 3 h. The samples were then once again washed thrice with PBST and subjected to rolling circle amplification by Phi29 DNA polymerase at 30 °C for overnight. After application of fluorescent detection probes in hybridization buffer, the samples were dehydrated with an ethanol series and mounted with mounting media. Images were captured, and signal dots were decoded to interpret RNA spatial position information [45].

Website construction and data acquisition.

To enhance communication and accessibility of our findings, we have made our results available through MSKCA [46]. Specifically, we developed the Ligament Cell Atlas (http://www.mskca.tech/Ligament/), which can be used to visualize our dataset. The data obtained from this study are stored in a MySQL database, which contains sample tissue details, library construction methods, cell numbers, expression matrices, and data visualization. To establish the necessary connection between the website (http://www.mskca.tech/Ligament/) and MySQL database, we utilized the PHP framework CodeIgniter. This framework allowed us to seamlessly implement various website functionalities. Furthermore, we incorporated JavaScript libraries, including jQuery (2.2.0) and jQuery labelauty, along with some additional plugins, to enable dynamic web services. Lastly, we used the R language ShinyCell package to create an additional webpage dedicated to visualizing our study data [47,48].

3. Results

3.1. HE and MASSON staining

Tissue samples of the abnormal ligamentum teres were collected from six patients with DDH; these samples were obtained during open reduction surgery, following specific inclusion and exclusion criteria (Table S1, Figs. S9).

All samples were subjected to both HE and MASSON staining. Pathological staining of the ligamentum teres revealed several changes, including focal fibrous tissue hyperplasia, obvious fibrous collagenization, local fasciculation, focal myxoid degeneration, reduced elastic fiber count, hyaline degeneration, and fatty degeneration in some regions (Fig. 1b and c, Fig. S9).

3.2. Cell-type annotation

To investigate transcriptome changes in different cell types within the ligamentum teres, we subjected four ligamentum teres samples to snRNA-Seq (Fig. 1a). We performed quality control on all samples using the Seurat package, resulting in 22,884 high-quality cells. Subsequently, we performed biological annotations based on differential gene expression within each cluster, established marker genes of cell types from published articles, and performed functional enrichment analysis. Consequently, six cell types were annotated: receptor-like cells (*CNTNAP2* [49], *PCDH15* [49], *EYS* [49], and *PTPRD* [49]); endotheliocytes (*PECAM1* [50] and

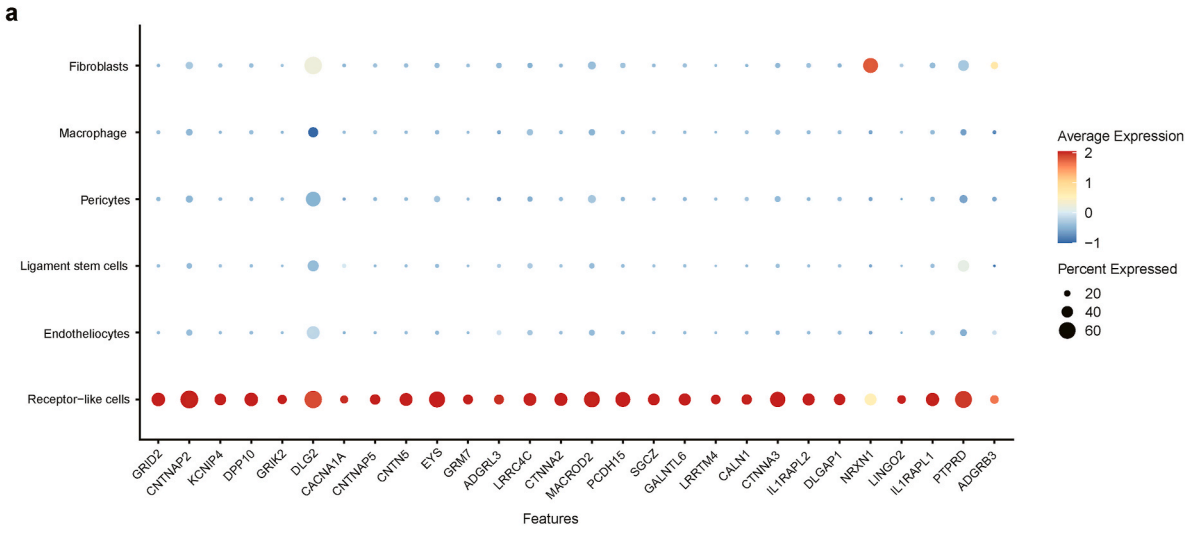

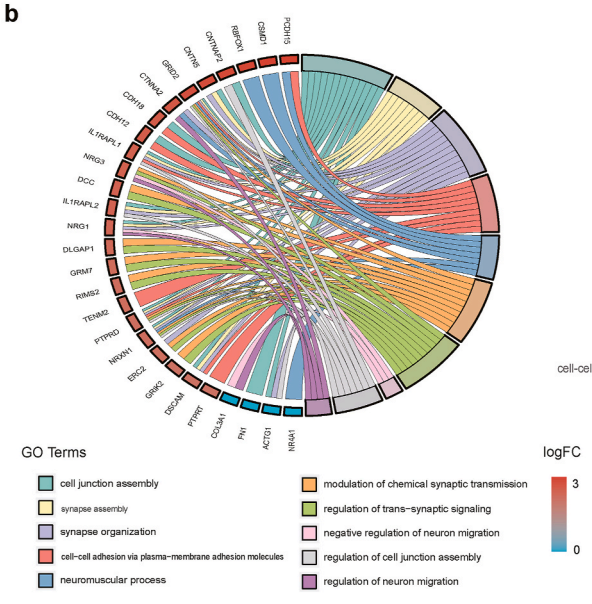

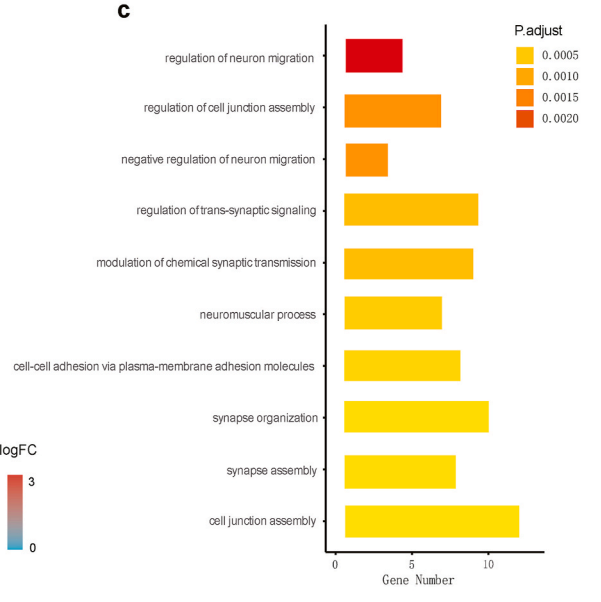

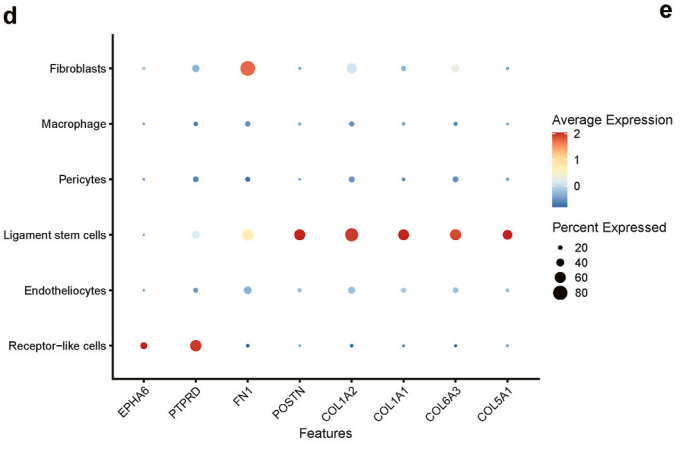

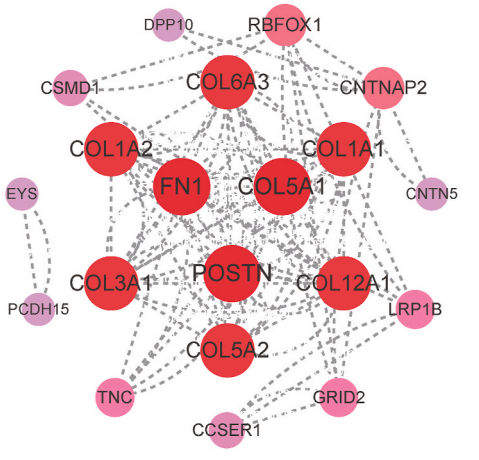

(caption on next page)

Fig. 2. Differential gene expression and gene sets enrichment analysis of cell types.
(a) Bubble plot illustrating the expression of neural molecule, synaptic regulatory, and ion channel genes in receptor-like cells. Circle color represents the average gene expression scale in different cell types, and circle size represents the proportion of genes expressed in different cell types.
(b) Circle diagram showing the relationship between genes enriched in receptor-like cells and each GO term. The color of each GO term is indicated below the graph. The logFC value represents the degree of gene expression, with darker colors indicating higher enrichment and expression levels.
(c) Bar graph displaying the GO terms enriched in receptor-like cells. Color shade represents adjusted p-value.
(d) Bubble plot showing the expression of eight differentially expressed DDH-associated genes in different cell types. Circle color represents the average gene expression scale in different cell types, and circle size represents the proportion of genes expressed in different cell types.
(e) PPI interaction network of differential genes in ligament stem cells. (For interpretation of the references to color in this figure legend, the reader is referred to the Web version of this article.)

VWF [50]); ligament stem cells [*COL1A1* [51], *CADM1* [51], and paired related homeobox 1 (*PRRX1*) [52,53]]; pericytes (*MCAM* [50]); macrophages (*PTPRC* [54],*CD86* [54], and *CD163* [54]); and fibroblasts (*FN1* [55] and *DCN* [55]). (Fig. 1d–f)

Furthermore, we obtained single-cell data of mouse ligaments from GSE194427 and performed cell-type annotation using the aforementioned analysis method. This analysis resulted in the annotation of eight cell types: macrophages (*Cd163* [54], *Cd68* [54], and *C1qa* [54]); ligament stem cells (*Prrx1* [52,53], *Fn1* [52,53], and *Dcn* [52,53]); neutrophils (*Csf3r* [22] and *Lcn2* [22]); erythroblasts (*Hba−a1* [22], *Hba−a2* [22], *Mki67* [22], and *Top2a* [22]); $CD8^+$ T cells (*Cd3d* [22] and *Cd8a* [22]); pericytes (*MCAM* [50]); endotheliocytes (*PECAM1* [50]); and B cells (*Cd19* [22] and *Ms4a1* [22]). (Fig. S1 b-c)

3.3. Gene expression comparison

To compare gene expression across different cell types, we utilized the FindAllMarks function (Seurat). Genes that were differentially expressed among cell types, with corrected p-value ≤ 0.05 and $|\text{logFC}| \geq 2$, were identified (Table S5). Receptor-like cells exhibited high expression of neural molecule genes, such as *LRRC4C*, *CTNNA2*, and *GRID2*, as well as ion channel-encoding genes, such as *KCNIP4* and *GRM7* [49](Fig. 2a).To understand the BPs and molecular functions associated with differentially expressed genes in receptor-like cells, we performed BP functional enrichment analysis, which revealed significant enrichment of several BPs, such as synapse assembly, modulation of chemical synaptic transmission, regulation of neuron migration, and neuromuscular process (Fig. 2b and c).

3.4. Expression of DDH-associated genes

Using the criteria of corrected p-value ≤ 0.05 and $|\text{logFC}| \geq 2$, we identified eight differentially expressed DDH-associated genes. Bubble plots were generated to visualize the expression of these genes across different cell types (Fig. 2d). Among them, neural molecule genes (*EPHA6* and *PTPRD*) were mainly highly expressed in receptor-like cells, while ECM genes (*FN1, POSTN, COL1A2, COL1A1, COL6A3,* and *COL5A1*) were mainly highly expressed in ligament stem cells (Fig. 2d). To further explore the potential biological functions of ligament stem cells, we constructed a PPI network using genes that were differentially expressed in ligament stem cells [40]. Within this network, *FN1, POSTN*, and *COL5A1* emerged as central genes with the highest node degrees, indicating their potential relevance to DDH (Fig. 2e).

3.5. Gene set enrichment analysis

To evaluate the potential metabolism-related biological functions of different cell types, we collected a metabolic gene set (Table S2) from a study by Wu et al. [25].Gene set enrichment analysis was then performed (Fig. 3a and c; Figs. S2a–5a), revealing the enrichment of gene sets related to sugar metabolism (e.g., glucose metabolism, glycogen metabolism, amino sugar and nucleotide sugar metabolism) and amino acid metabolism (e.g., phenylalanine, tyrosine, and tryptophan biosynthesis and phenylalanine and tyrosine metabolism). Moreover, gene sets related to lipid metabolism (e.g., triglyceride metabolism, linoleic acid metabolism, and fatty acid biosynthesis) were enriched in receptor-like cells and ligament stem cells (Fig. 3a and c). These results suggested that energy metabolism plays a key role in maintaining the biological functions of receptor-like cells and ligament stem cells.

To comprehensively characterize the biological functions of different cell types beyond metabolism, we collected KEGG gene sets (Table S3) from MSigDB [26,27] and performed gene set enrichment analysis. Receptor-like cells were primarily enriched in pathways such as neuroactive ligand–receptor interaction, neurotrophin signaling pathway, and ECM–receptor interaction, while ligament stem cells were mainly enriched in pathways such as neuroactive ligand–receptor interaction, ECM–receptor interaction, and TGF-beta signaling pathway (Fig. 3).

3.6. Pseudotemporal analysis

We used the Monocle package to perform pseudotemporal analysis on ligament stem cells, fibroblasts, and pericytes (Fig. 5a, 5b). Box plots were generated to illustrate the differentiation status of cells within six different subpopulations, indicating a range from poorly to highly differentiated cells, with pericytes exhibiting the least differentiation (Fig. S9a). Further, pericytes were found to represent the starting point of the cell trajectory and branched into two main branches. Ligament stem cells and fibroblasts occupied the opposite ends of these branches, representing two terminally differentiated cell types (Fig. 5c and d). Through the BEAM function

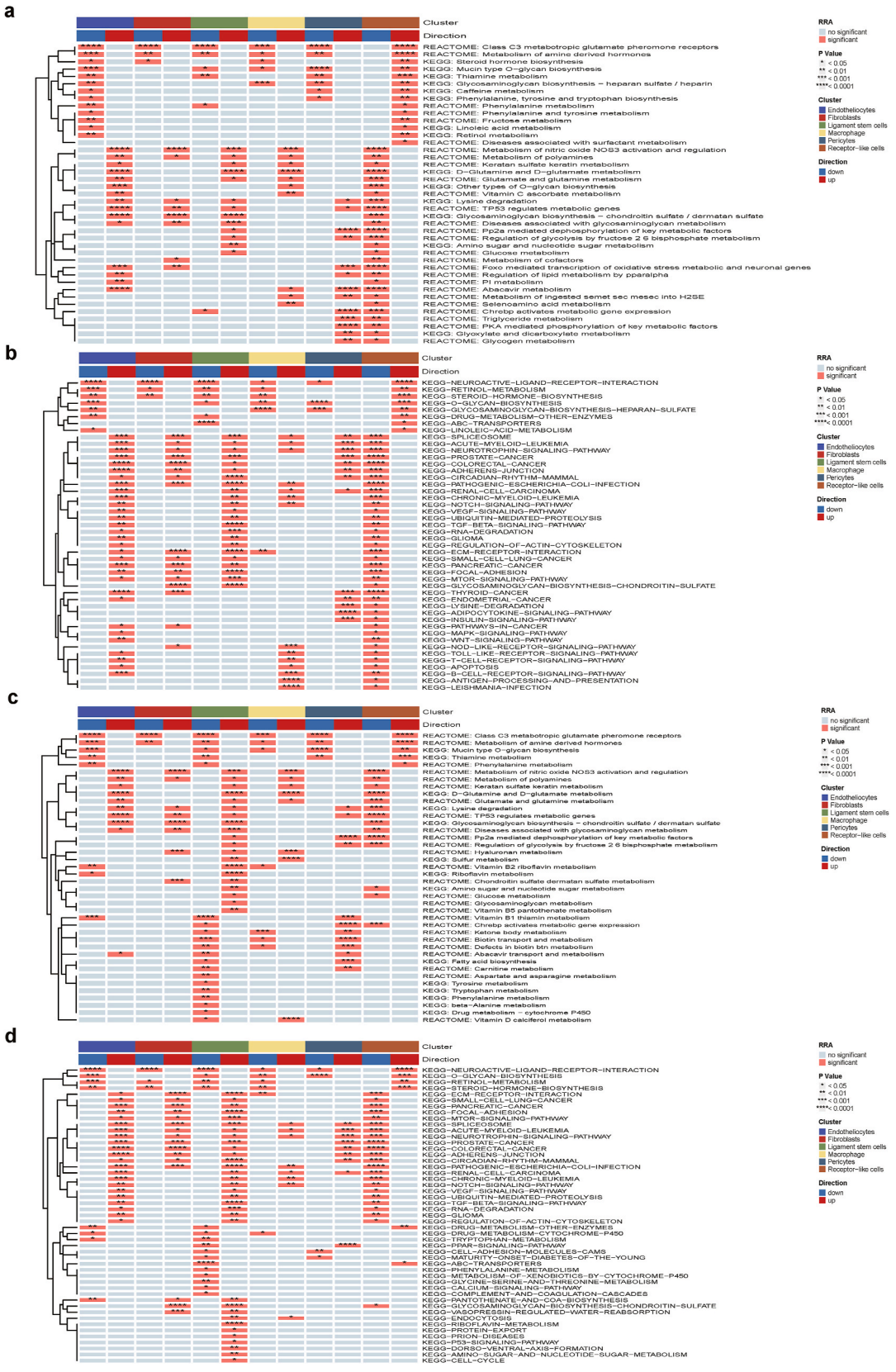

(caption on next page)

Fig. 3. Gene sets enrichment analysis of cell types(a–b) Heatmaps displaying all statistically significant metabolic-related and KEGG gene sets in receptor-like cells, respectively.
(c–d) All statistically significant metabolic-related and KEGG gene sets in ligament stem cells.
The blue grid indicates that the enrichment or non-enrichment of the gene set in this cell type is not statistically significant. The red grid indicates that the enrichment or non-enrichment of the gene set in the cell type is statistically significant. The number of asterisks in the red grid indicates the p-value of the grid: * represents $p < 0.05$, ** represents $p < 0.01$, *** represents $p < 0.001$, and **** represents $p < 0.0001$.
The clustering tree on the left of the heatmap represents the similarity of enrichment patterns of different gene sets in different cell subpopulations. Two types of bar graphs are evident above the heatmap. In the bar chart near the heatmap, blue indicates that the gene set is not enriched, and red indicates that the gene set is enriched. In the bar charts away from the heatmap, different colors represent different cell subpopulations. Blue in the Direction part represents downregulation, while red represents upregulation. (For interpretation of the references to color in this figure legend, the reader is referred to the Web version of this article.)

(q-value $< 1e{-}4$, $p < 1e{-}4$), we identified 656 differentiation-related genes, which were further clustered into six groups using the plot_genes_branched_heatmap function (with the ward.D2R clustering method) (Table S6). Subsequently, GO-BP enrichment analysis was performed on these clusters using the clusterProfiler R package, and statistically significant GO terms (p-adjust ≤ 0.05) were identified (Table S7).

The ECM plays an essential role in the differentiation process of stem cells [56]. Therefore, we collected 864 ECM-related genes (Table S8) [57] from previous studies and visualized their expression along the pseudotemporal trajectory (Fig. 6). The genetic heatmap revealed that response to peptide, response to peptide hormone, and response to oxidative stress pathways were primarily enriched in pericytes at the initiation point of differentiation. The highly expressed gene clusters during the differentiation of pericytes to ligament stem cells are C4, C5, and C6, such as *ECM2, COL5A1, ASPN,* and other genes. Among these clusters, the average expression values of genes in C4 and C5 exhibited an increasing trend, while those of genes in C6 initially decreased and then increased. Further, GO-BP enrichment analysis revealed enrichment in processes such as ECM organization, chondrocyte differentiation, and collagen fibril organization. During the differentiation process from pericytes to fibroblasts, highly expressed gene clusters (C1 and C2) included various genes, such as *SNED1, SEMA3A, PRG4,* and S100A4. The average gene expression values of genes in C1 and C2 generally increased, whereas those of genes in C3 showed a downward trend. GO-BP enrichment analysis indicated enrichment in processes such as axonogenesis, axon development, and neuron projection guidance (Fig. 5e).

3.7. Construction of an intercellular communication network

Cellular communication is a fundamental BP that plays a crucial role in tissue function. Elucidating the intercellular communication network provides insights into information transfer and exchange between cells at a cellular level. To gain a better understanding of the interactions among different cell subpopulations in the ligamentum teres, we used the CellChat R package (v1.1.3) [44] to infer and visualize the intercellular communication network. Chord diagrams were plotted to depict the statistically significant distribution of ligand–receptor pairs in different cell types, and bubble plots were used to visualize the interaction of all statistically significant ligand–receptor pairs within specific signaling pathways of interest across different cell types. Overall, 154 interactions were identified, implying extensive crosstalk between different cell types within the ligamentum teres. These interactions encompassed 45 types of ligand–receptor pairs and 18 signaling pathways (Fig. 4a).

To identify ligand–receptor pairs associated with DDH pathogenesis, we intersected ligand–receptor pair genes with differentially expressed DDH-associated genes. This yielded eight ligand–receptor pairs: *FN1–CD44, FN1–(ITGAV + ITGB8), COL1A2–CD44, COL1A1–CD44, COL1A1–(ITGAV + ITGB8), COL1A2–(ITGAV + ITGB8), COL6A3–CD44, and COL6A3–(ITGAV + ITGB8)* (Fig. 4b–i). These pairs were closely related to the ECM–receptor pathway. The interactions between ligament stem cells and fibroblasts significantly enriched these ligand–receptor pairs. Among them, *COL1A1–(ITGAV + ITGB8)* was found to exclusively exist in the interaction between ligament stem cells and fibroblasts. Chord diagrams highlighted the specific distribution of these ligand–receptor pairs among different cell types. It is notable that the *PTPRM–PTPRM* ligand–receptor pair existed in most cell interactions, with the interaction being more pronounced when endotheliocytes were used as receptor cells or ligand cells (Fig. 4).

3.8. MiP-Seq

MiP-Seq is an efficient approach for spatial and multiomics analyses, providing a spatial landscape of DNA, RNA, proteins, and small biomolecules (neurotransmitters) at subcellular resolution [45]. To identify the cellular heterogeneity of the ligamentum teres at the spatial transcriptome level, the expression distribution of marker genes in different cell types within the ligamentum teres were determined with MiP-Seq (Fig. 6a–g). Moreover, we investigated the expression distribution of differentially expressed DDH-associated genes in the ligamentum teres at the spatial level using MiP-Seq (Fig. 6h–m). Clustering ligamentum teres cells at the spatial level based on MiP-Seq led to the identification of ligament stem cells, fibroblasts, pericytes, and endotheliocytes (Fig. 6n). On determining DDH-associated gene expression levels in different cell types, we found evidence at the spatial level supporting the role of ligament stem cells in DDH occurrence and progression (Fig. 6o).

3.9. Website construction and data acquisition

To facilitate communication and dissemination of our findings, we have deposited our data on MSKCA (http://www.mskca.tech/

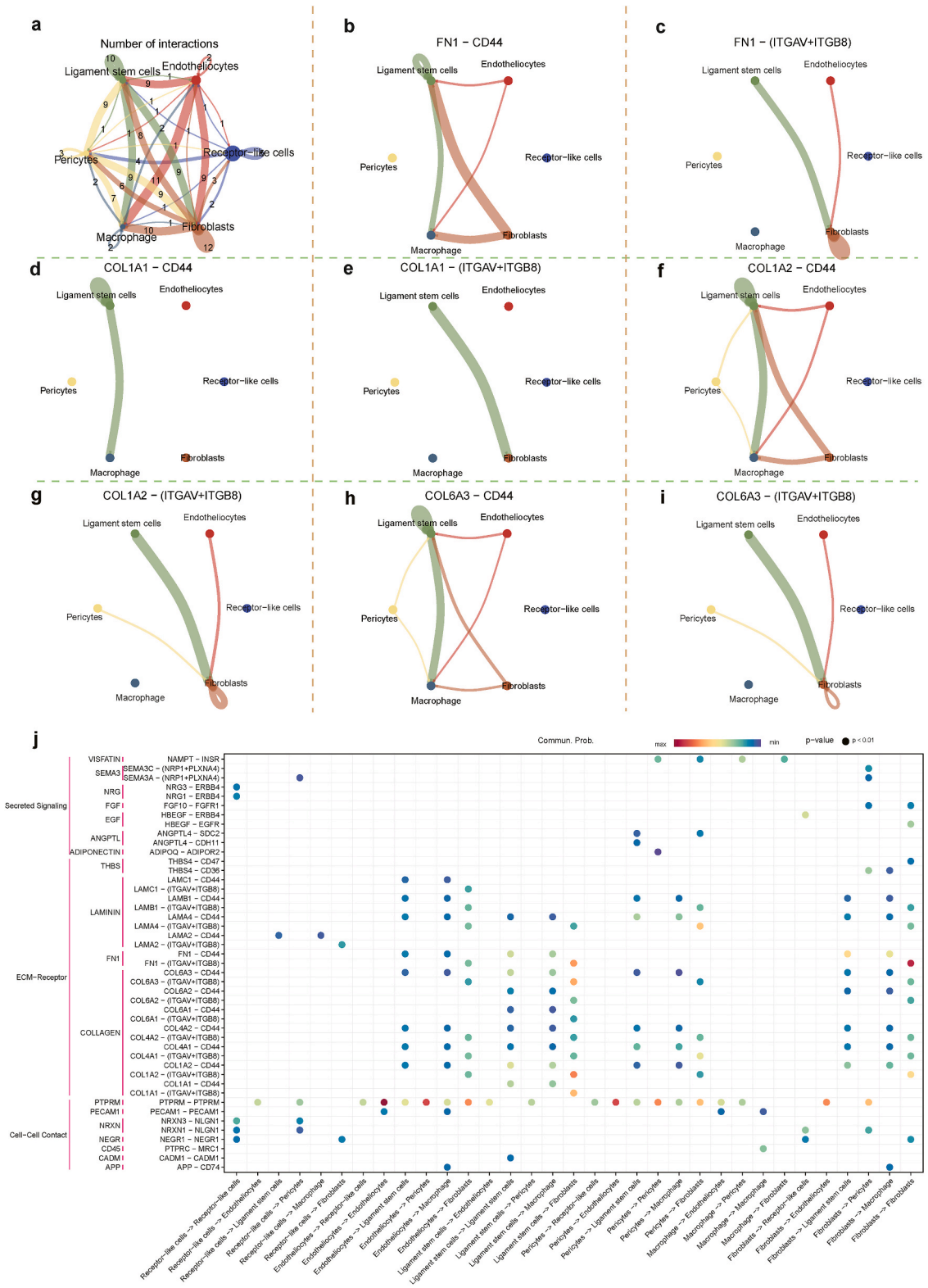

Fig. 4. Communication network of different cell types.
(a) Chord diagram showing the communication network between different cell types within the ligamentum teres, representing the number of direct interaction pairs among different cells.
(b–i) Chord diagrams showing the expression of the following ligand–receptor pairs in different cell types: *FN1–CD44, FN1–(ITGAV + ITGB8),*

COL1A2–CD44, COL1A1–CD44, COL1A1–(ITGAV + ITGB8), COL1A2–(ITGAV + ITGB8), COL6A3–CD44, and COL6A3–(ITGAV + ITGB8).
(j) Bubble plot showing the proportion and significance of each ligand–receptor interaction pair in different cellular interactions. Circle color represents the proportion and circle size represents the significance of the interaction pair in that cell interaction.

Ligament/). Interactive visualizations are available on this website, designed to help users efficiently use our data to explore gene expression and better understand our study findings. The online database predominantly includes Search and Download functions (Fig. S6a). Users can enter genes of interest in the Search interface (Fig. S6b), and gene expression levels will be displayed in different cell types. By hovering over the results, users can view the gene expression value in different cell types (Fig. S6c). The online database contains a ShinyCell link, which primarily includes seven modules: CellInfo vs. GeneExpr, CellInfo vs. CellInfo, GeneExpr vs. GeneExpr, Gene coexpression, Violinplot/Boxplot, Proportion plot, and Bubbleplot/Heatmap (Fig. S7a). In the first four modules, the UMAP cluster diagram is mainly used as the benchmark, allowing users to selectively display data of a certain orig.ident or cell type. In the CellInfo vs. GeneExpr module, users can view gene expression in different orig.ident or cell types (Fig. S7b). In the CellInfo vs. CellInfo module, users can simultaneously view the distribution of different cell types (Fig. S7c). In the GeneExpr vs. GeneExpr module, the expression of two genes of interest in different cell types is simultaneously displayed through two clustering diagrams (Fig. S8a). Similarly, in the Gene coexpression module, the expression of two genes of interest in different cell types is simultaneously displayed in the same clustering diagram; moreover, the expression ratio of coexpressed gene can be obtained (Fig. S8b). The Violinplot/Boxplot module allows users to visualize the distribution of nCount_RNA and nFeature_RNA for different cell types using a violin or box plot (Fig. S8c). Finally, in the Bubbleplot/Heatmap module, users can simultaneously view the expression of several genes in different cell types or under different orig.ident (Fig. S8d). Figures or tables generated by each module can be downloaded as needed.

4. Discussion

DDH is a common hip disease in pediatric orthopedics. While some infants have mild hip dysplasia that resolves on its own, untreated hip deformities can progressively worsen and lead to muscle stiffness, pain, limited joint motion, and eventually degenerative osteoarthritis in adulthood [58]. The ligamentum teres is a crucial structure in the hip joint and evidently plays a key role in joint stabilization, similar to the anterior cruciate ligament in the knee [59]. Damage or laxity of the ligamentum teres can cause hip instability, dyskinesia, and hip dislocation [59]. To investigate the cellular heterogeneity of the ligamentum teres and clarify its pathogenic mechanism in DDH, we, for the first time, performed snRNA-Seq to create a single-cell map of the abnormal ligamentum teres in patients with DDH. We identified six cell types: receptor-like cells, endotheliocytes, ligament stem cells, pericytes, macrophages, and fibroblasts. To validate the conserved heterogeneity of ligament cells across species, we compared the transcriptomes of human and mouse ligament cells by reanalyzing scRNA-Seq data from a recent mouse study and found that most of the cell clusters in human ligaments were also present in mouse ligaments, indicating conservation of gene expression in different cell types, including macrophages, ligament stem cells, and pericytes (Figs. S1b–c).

Proprioception plays an essential role in body balance maintenance, movement coordination, and muscle strength regulation [60]. Proprioceptive deficits may be related to the pathogenesis of musculoskeletal diseases, such as adolescent idiopathic scoliosis [61]. Receptor-like cells seem to be closely associated with the proprioception of the ligamentum teres. The presence of blood vessels, nerves, and mechanoreceptors (Pacinian corpuscles and free nerve endings) in the ligamentum teres suggests that it provides information on joint position and motion direction through its nerves and proprioceptors. Mechanoreceptors transmit information to neurons by sensing mechanical stimuli and converting them into electrical signals, a process involving ion channels [62]. We found receptor-like cells to highly express neural molecule genes, synaptic regulatory genes (e.g., *LRRC4C, CTNNA2, and GRID2*), and ion channel genes (e.g., *KCNIP4 and GRM7*). Further, differential genes in receptor-like cells were enriched in BPs related to nerve and synapse regulation (*EPHA6* and *PTPRD*), supporting their potential role in proprioception (Fig. 2a–d). Collectively, our results suggested that receptor-like cells are closely related to the occurrence of DDH.

Fibroblasts, in addition to producing connective tissues, serve as progenitors for specialized mesenchymal cell types [63]. We defined a subset of fibroblasts expressing *PRRX1*$^{+}$ and *CADM1*$^{+}$ stemness genes as ligament stem cells. *PRRX1* is a mesodermal transcription factor that promotes the differentiation of mesenchymal precursors [64]. Qin et al. [65] identified a population of antler blastema progenitor cells that originated from PRRX1^{+} mesenchymal cells in deer antlers and directed the antler regeneration process. Wilk et al. [53] identified a population of *PRRX1*$^{+}$ skeletal stem cells expressed only in skull sutures and vital for bone formation. In addition, a group of skeletal stem cells (*PDGFRA*$^{low/-}$*PDPN*$^{+}$ *CADM1*$^{+}$) has been reported to exhibit the potential of self-renewal and differentiation into cartilage and osteoblasts [52].

The structure of the hip joint is complex, and the anatomical and pathological characteristics of DDH include bones and soft tissues, such as the acetabulum, femoral head, and other bone tissues, as well as soft tissues, such as the labrum, ligamentum teres, and joint capsule. Wynne-Davies R et al. [66] believe that there may be two inheritance patterns in the pathogenesis of DDH. One is a multi-gene system that regulates acetabular cartilage or bone development. The other is a multi-gene system that regulates the development of surrounding soft tissues such as the hip joint capsule and ligamentum teres. The meta-analysis results of Kenanidis E et al. [36] show that current genetic research on DDH is mainly focused on chromosomes 1, 3, 12, 17, and 20. The genes closely related to DDH disease mainly include CX3CR1, GDF5, and COL1A1. Among them, the single nucleotide polymorphism at the rs143384 site of the GDF5 gene on chromosome 20 is most closely related to the phenotype of DDH. GDF5 is closely related to the growth and development of bone and cartilage and the formation process of joints. However, pathological changes in the hip joint capsule and ligamentum teres caused by collagen metabolism disorders are also one of the causes of DDH [67]. Collagen is an essential structural protein in connective tissue.

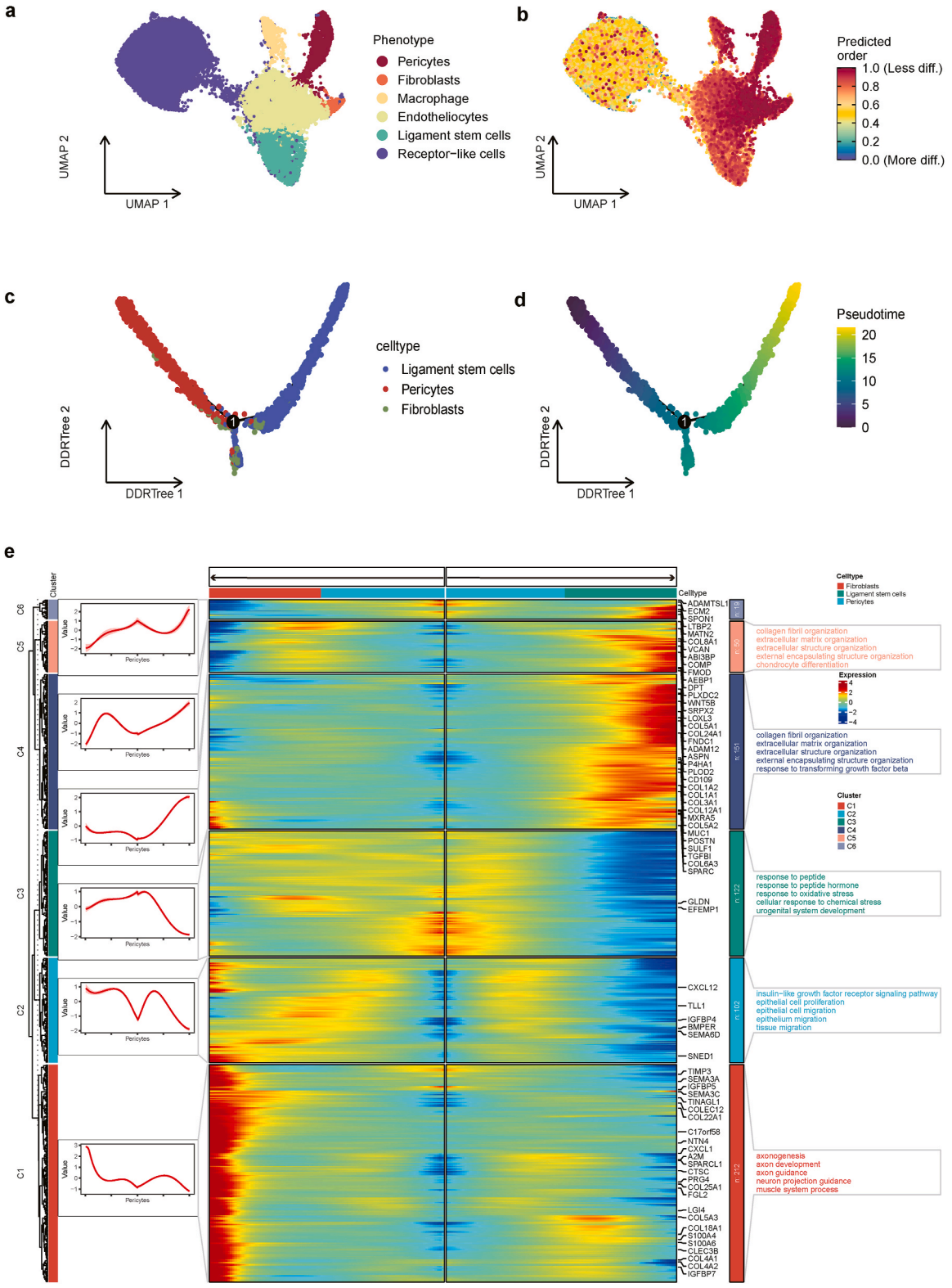

Fig. 5. Atlas and trajectory analysis of ligamentum teres.
(a–b) UMAP plots depicting the degree of differentiation of different cell types. Redder colors indicate lower and bluer colors indicate higher degrees of differentiation
(c-d) DDRtree diagram showing the distribution of ligament stem cells, pericytes, and fibroblasts on the pseudo-chronological trajectory.

(e) Heatmap showing the expression of 656 differentiation-related genes along pseudotemporal trajectories. The clustering tree and bar graph on the left divide these genes into six clusters. The line graph on the left represents the overall expression trend of genes in different clusters. The heatmap in the middle represents the expression of differentiation-related genes along the pseudotemporal trajectory, with ECM-related genes highlighted. The bar graphs and annotations on the right represent the enriched GO-BP terms in the top four clusters.

COL1A1 and COL1A2 mainly encode type I collagen. Therefore, COL1A1 and COL1A2 gene mutations may affect the stability of the molecular structure of type I collagen, which can cause the connective tissue to lose its tensile resistance [68]. In addition, Zhao L et al. [68] conducted mutation screening in the promoter region of the COL1A1 gene and detected three mutations in the COL1A1 gene promoter in 10 DDH patients. In this study, we observed that ECM-related differentially expressed DDH-associated genes (*FN1, POSTN, COL1A2, COL1A1, COL6A3,* and *COL5A1*) were highly expressed in ligament stem cells (Fig. 2d), indicating a potential close relationship between ligament stem cells and DDH. To validate and understand the spatial expression patterns of these genes in the ligamentum teres, we performed MiP-Seq, which confirmed the findings of single-cell sequencing at the spatial level (Fig. 6). To gain further insights into the potential biological functions of ligament stem cells, we constructed a PPI network using STRING. Among the differential genes in ligament stem cells, *FN1, POSTN,* and *COL5A1* showed the highest node degrees, suggesting that they have significant implications in DDH (Fig. 2e). Moreover, metabolic-related and KEGG gene set enrichment analyses of ligament stem cells revealed enrichment in pathways associated with lipid metabolism and ECM regulation (Fig. 3c and d). We believe that abnormal lipid metabolism and dysregulation of ECM-related pathways can lead to excessive accumulation of fat and ECM in the ligamentum teres, leading to its thickening and hypertrophy.

By constructing the intercellular communication network of different cell types in the ligamentum teres, we observed a close interaction between various cell subpopulations. Through the intersection of ligand–receptor pair genes and differentially expressed DDH-associated genes, we found eight ligand–receptor pairs that might be implicated in DDH pathogenesis. These ligand–receptor pairs were found to be closely related to the ECM–receptor pathway and showed significant enrichment in the interaction relationship between ligament stem cells and fibroblasts. These results suggest that ligament stem cells and fibroblasts play a regulatory role in ECM-related pathways, contributing to pathological thickening and hypertrophy of the ligamentum teres.

Furthermore, we observed the existence of the *PTPRM–PTPRM* ligand–receptor pair in most cell interactions, with enhanced interaction when endotheliocytes were used as receptor cells or ligand cells (Fig. 4j). The protein encoded by *PTPRM* belongs to the protein tyrosine phosphatase family, and receptor protein tyrosine phosphatases have been known to mediate homotypic cell–cell interactions and regulate p120 catenin/CTNND1 phosphorylation, which is involved in adipogenic differentiation [69,70]. Tang et al. [71] reported that endothelial cells actively regulate fat function, impacting whole-body metabolic processes. Furthermore, Crewe et al. [72] found, in the context of metabolic regulation, that small extracellular vesicles mediate a form of intercellular communication within adipose tissue, contributing to multifaceted crosstalk between adipocytes and endothelial cells. Herein HE staining findings revealed more fatty degeneration (black arrow) in the ligamentum teres (Fig. 1b). Overall, these results suggest that endotheliocytes promote adipocyte deposition through *PTPRM* and other signaling pathways, potentially contributing to ligamentum teres thickening and hypertrophy.

Pericytes, which are blood vessel wall cells located on the outside of capillaries, exhibit self-renewal properties and can migrate to develop myofibroblast properties, leading to excessive ECM deposition [57]. They can also differentiate into multipotent adult stem cells, contributing to tissue repair and regeneration [73]. Prior studies have indicated that pericytes, found in the vasculature of tendons, can serve as a potential source of progenitor cells for adult tendon fibroblasts [50]. In this study, we found that pericytes can potentially differentiate into ligament stem cells and fibroblasts (Fig. 5c and d). Fibroblasts play a key role in ECM synthesis, participating in connective tissue formation via the deposition of various components, including collagens, proteoglycans, elastin, fibronectin, microfibrillar proteins, and laminins, which together form the microsome [63]. In addition, fibroblasts “tug and pull” on their ECM, resulting in tissue-level mechanical forces and matrix polarization and contributing to tissue-specific microsomes and tissue mechanics [63,74]. Considering that the ECM plays a pivotal role in the differentiation process of stem cells [56], we analyzed 864 ECM-related genes collected from previous studies and investigated their expression along the pseudotemporal trajectory (Fig. 5, Table S8) [57].

In addition, we found that endotheliocytes are enriched in VEGF-SIGNALING-PATHWAY through KEGG gene sets enrichment analysis (Fig. S2). Fibroblasts, pericytes, and endotheliocytes are enriched in the Foxo-mediated transcription of oxidative stress metabolic and neuronal genes pathways (Fig. S2, Fig. S3, and Fig. S5). We also found that macrophages enriched NEUROTROPHIN−SIGNALING−PATHWAY. In addition, through cell communication, we found that three ligand–receptor pairs related to NEUROTROPHIN exist in the communication between pericytes, receptor-like cells, and fibroblasts. SEMA3A − (NRP1+PLXNA4) interaction mediates communication between receptor-like cells and pericytes. Communication between fibroblasts and pericytes is mediated by SEMA3A − (NRP1+PLXNA4) and SEMA3C − (NRP1+PLXNA4) interactions (Fig. 4j). Endotheliocytes are a significant source of vascular heterogeneity in different tissues and a primary source of transcriptional changes in multiple disease states. Endothelial cells line the interior of all blood and lymphatic vessels and play a key role in transporting oxygen and nutrients, regulating blood flow, regulating immune cell trafficking, and maintaining tissue homeostasis. VEGF and Notch signaling pathways are critical regulatory systems in blood vessel development [75]. In this study, we found the presence of many blood vessels in ligamentum teres through HE staining (Fig. S9). Perumal V et al. [76] also found neurovascular structures in ligamentum teres. In osteoarthritis, studies have confirmed that abnormal blood vessels and innervation may be the pathogenesis of OA. Wang Hs et al. [77] found that the levels of neuropeptides and inflammatory cytokines in the synovial tissue and fluid of DDH patients were significantly increased, but the relationship with the pathogenesis of DDH is unclear. Although this study has not confirmed the role of blood vessels and nerves in the

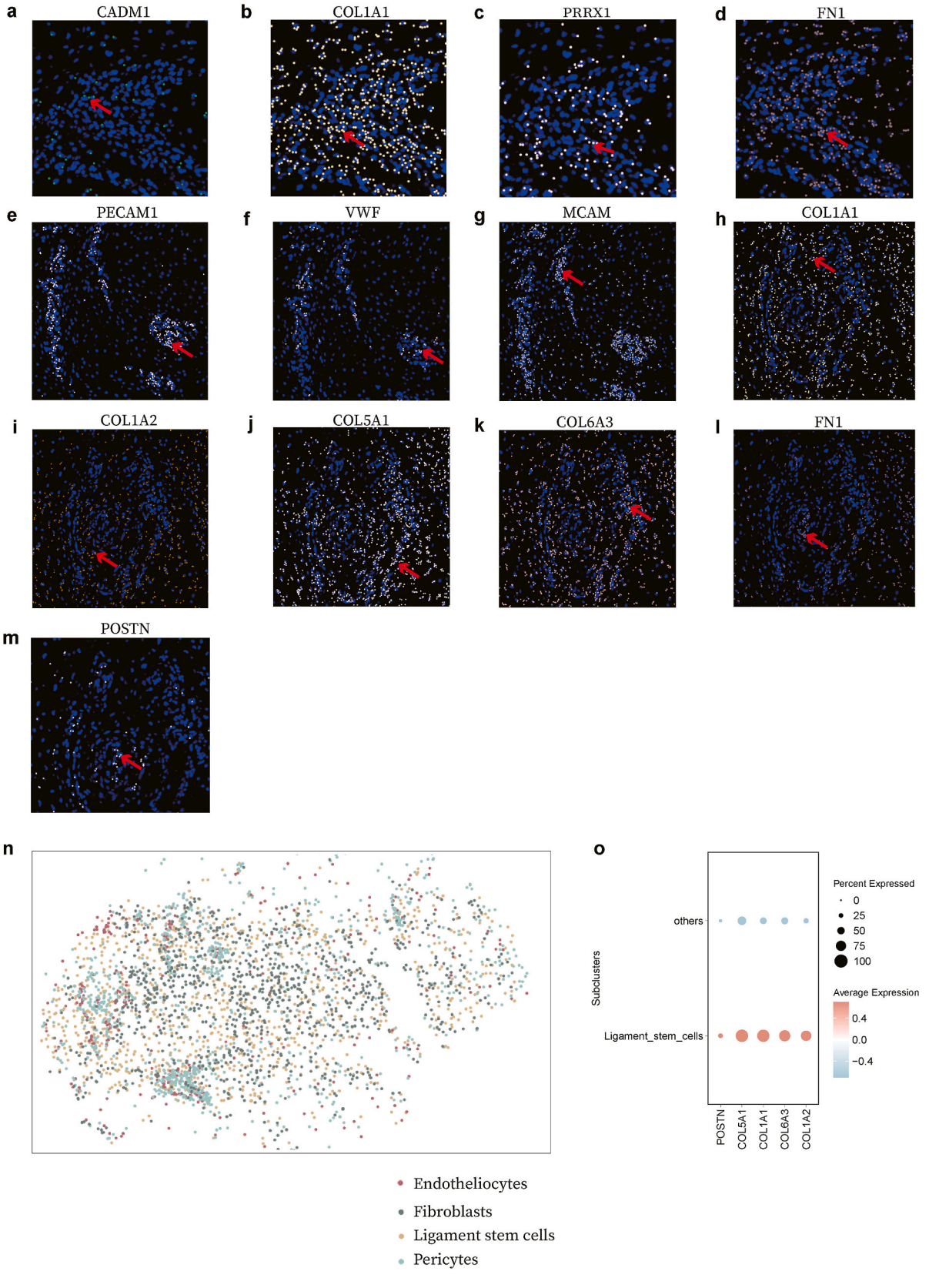

(caption on next page)

Fig. 6. MiP-Seq results
(a–c) Spatial transcriptome map of the expression of three marker genes *(CADM1, PRRX1, and COL1A1)* in ligament stem cells.
(d)Spatial transcriptome map of the expression of a marker gene (*FN1*) in fibroblasts.
(e–f) Spatial transcriptome map of the expression of two marker genes (*PECAM1* and *VWF*) in endotheliocytes.
(g)Spatial transcriptome map of the expression of a marker gene (*MCAM*) in pericytes.
(h–m) Spatial transcriptome map of DDH-associated genes (*COL1A1, COL1A2, COL5A1, COL6A3, FN1, and POSTN*) differentially expressed in different cell types within the ligamentum teres.
(n)Scatterplot showing the spatial distribution of different cell types within the ligamentum teres.
(o)Bubble plot illustrating differences in the expression of differentially expressed DDH-associated genes (*COL1A1, COL1A2, COL5A1, COL6A3, FN1, POSTN*) in ligament stem cells and other cell populations.

pathogenesis of DDH, it provides a new idea for exploring the pathogenesis of DDH.

This study has certain limitations. First, we have no normal control of ligamentum teres. We could not compare and identify changes in individual cell populations and differences in gene expression between normal and disease states. In addition, the DDH-related genes included in this study may only partially represent the key factors in the pathogenesis of DDH. The relevant sites detected by genome-wide association studies and whole-exome sequencing are usually located in intergenic regions, so it is difficult to determine which candidate gene is related to DDH. Moreover, studies have shown that multiple genes may influence a single genomic locus, further confounding candidate gene selection [78]. In addition, other candidate genes may not be included in this study. However, these are limitations common to the field. In addition, our sample size is relatively small, and we expect to collect more samples through multicenter studies. Despite this, our results provide new insights and ideas to understand the pathogenic mechanism of the ligamentum teres in DDH. Our study will serve as a valuable resource for constructing a comprehensive cell atlas for human musculoskeletal diseases, potentially becoming a basis for diagnostics, monitoring, and treating musculoskeletal diseases.

5. Conclusions

For the first time, we elucidated the cellular heterogeneity of the abnormal ligamentum teres in patients with DDH at the single-cell and spatial levels using snRNA-Seq and MiP-Seq, which allowed us to construct a single-cell map of the ligamentum teres. We found that receptor-like cells and ligament stem cells are closely associated with the pathogenesis of DDH. Moreover, ligament stem cells appear to be involved in the regulation of ECM metabolism and play an essential role in the pathological changes leading to ligamentum teres thickening and hypertrophy. Eight ligand–receptor pairs related to the ECM–receptor pathway were identified to be closely linked to DDH. Finally, we believe that pericytes in the ligamentum teres could potentially serve as a source of ligament stem cells and fibroblasts.

Ethics approval and consent to participate

This study was reviewed and approved by the ethics committee of our hospital (institutional review board approval no.: 202300202). Before conducting this study, the parents or guardians of the children were informed of the purpose of this study and signed an informed consent form.

Funding

This study was supported by Guangdong High-level Hospital Construction Fund (ynkt2022-zz09), Science and Technology Innovation Bureau of Luohu District(LX202302123) and Sanming Project of Medicine in Shenzhen (SZSM202011012).

Data availability statement

We have deposited our data on MSKCA (http://www.mskca.tech/Ligament/).

CRediT authorship contribution statement

Zhenhui Zhao: Writing – review & editing, Writing – original draft, Visualization, Investigation, Formal analysis, Data curation, Conceptualization. **Chuiqin Fan:** Writing – review & editing, Visualization, Validation, Formal analysis, Data curation, Conceptualization. **Shiyou Wang:** Visualization, Validation, Formal analysis, Data curation, Conceptualization. **Haoyu Wang:** Visualization, Methodology, Formal analysis, Data curation, Conceptualization. **Hansheng Deng:** Writing – original draft, Visualization, Software, Methodology. **Shuaidan Zeng:** Validation, Software, Methodology, Data curation. **Shengping Tang:** Writing – review & editing, Writing – original draft, Validation, Supervision, Conceptualization. **Li Li:** Writing – original draft, Visualization, Validation, Supervision, Data curation. **Zhu Xiong:** Writing – review & editing, Writing – original draft, Visualization, Data curation, Conceptualization. **Xin Qiu:** Writing – review & editing, Writing – original draft, Visualization, Validation, Supervision, Methodology, Formal analysis, Conceptualization.

Declaration of competing interest

The authors declare that they have no known competing financial interests or personal relationships that could have appeared to influence the work reported in this paper.

Acknowledgements

We would like to thank Gang Cao(Huazhong Agricultural University, Wuhan, China), and Zhihui Zhang, Keji Yan and Mingyuan Zheng(spatial FISH Ltd., Shenzhen, China) for their help. We would like to express gratitude to all the patients and their families. We also thank Dr. Jianming Zeng(University of Macau, Macau, China), and all the members of his bioinformatics team, biotrainee, for generously sharing their experience and codes.

Appendix A. Supplementary data

Supplementary data to this article can be found online at https://doi.org/10.1016/j.heliyon.2024.e27803.

References

[1] J. Han, Y. Li, Progress in screening strategies for neonatal developmental dysplasia of the hip, Frontiers in surgery 9 (2022) 995949.
[2] A.A. Simionescu, M.M. Cirstoiu, C. Cirstoiu, A.M.A. Stanescu, B. Crețu, Current evidence about developmental dysplasia of the hip in pregnancy, Medicina (Kaunas, Lithuania) 57 (7) (2021).
[3] S.K. Storer, D.L. Skaggs, Developmental dysplasia of the hip, Am. Fam. Physician 74 (8) (2006) 1310–1316.
[4] L. Li, K. Sun, L. Zhang, Q. Zhao, X. Cheng, Y. Dang, Heritability and sibling recurrent risk of developmental dysplasia of the hip in Chinese population, Eur. J. Clin. Invest. 43 (6) (2013) 589–594.
[5] E. Kenanidis, N.K. Gkekas, A. Karasmani, P. Anagnostis, P. Christofilopoulos, Tsiridis Ejtjoa, Genetic predisposition to developmental dysplasia of the hip 35 (1) (2020) 291–300. e291.
[6] A.A. Simionescu, M.M. Cirstoiu, C. Cirstoiu, A.M.A. Stanescu, B.J.M. Crețu, Current evidence about developmental dysplasia of the hip in pregnancy 57 (7) (2021) 655.
[7] J.G. O'Beirne, K. Chlapoutakis, S. Alshryda, U. Aydingoz, T. Baumann, C. Casini, M. de Pellegrin, G. Domos, B. Dubs, Hemmadi SjuidM-EjoU, International interdisciplinary consensus meeting on the evaluation of developmental dysplasia of the hip 40 (4) (2019) 454–464.
[8] S. Yang, N. Zusman, E. Lieberman, R.Y. Goldstein, Developmental dysplasia of the hip, Pediatrics 143 (1) (2019).
[9] J.G. O'Beirne, K. Chlapoutakis, S. Alshryda, U. Aydingoz, T. Baumann, C. Casini, M. de Pellegrin, G. Domos, B. Dubs, S. Hemmadi, et al., International Interdisciplinary Consensus Meeting on the evaluation of developmental dysplasia of the hip, Ultraschall der Med. 40 (4) (2019) 454–464 (Stuttgart, Germany : 1980).
[10] E. Ipplito, Y. Ishii, I.V. Ponseti, Histologic, histochemical, and ultrastructural studies of the hip joint capsule and ligamentum teres in congenital dislocation of the hip, Clin. Orthop. Relat. Res. (146) (1980) 246–258.
[11] N. Kaku, T. Shimada, T. Tabata, H. Tagomori, T. Abe, J.J. Zhang, H. Tsumura, Three-dimensional architecture of the ligamentum teres in the human hip joint, Muscles, ligaments and tendons journal 7 (3) (2017) 442–448.
[12] D. Jovic, X. Liang, H. Zeng, L. Lin, F. Xu, Y. Luo, Single-cell RNA sequencing technologies and applications: a brief overview, Clin. Transl. Med. 12 (3) (2022) e694.
[13] J.E. Rood, A. Maartens, A. Hupalowska, S.A. Teichmann, A. Regev, Impact of the human cell atlas on medicine, Nature medicine 28 (12) (2022) 2486–2496.
[14] J.L. Cummings, A.K. Oladeji, S. Rosenfeld, M. Johnson, R. Goldstein, G. Georgopoulos, L. Stephenson, N.W. White, P. Hosseinzadeh, Outcomes of open reduction in children with developmental hip dislocation: a multicenter experience over a decade, Journal of pediatric orthopedics 43 (6) (2023) e405–e410.
[15] C. Liu, T. Wu, F. Fan, Y. Liu, L.J.C.S.H.L. Liu, A Portable and Cost-Effective Microfluidic System for Massively Parallel Single-Cell Transcriptome Profiling, 2019.
[16] P. Hu, E. Fabyanic, D.Y. Kwon, S. Tang, Z. Zhou, H. Wu, Dissecting cell-type composition and activity-Dependent transcriptional state in Mammalian Brains by Massively parallel single-nucleus RNA-seq, Molecular cell 68 (5) (2017) 1006–1015.e1007.
[17] N. Habib, I. Avraham-Davidi, A. Basu, T. Burks, K. Shekhar, M. Hofree, S.R. Choudhury, F. Aguet, E. Gelfand, K. Ardlie, et al., Massively parallel single-nucleus RNA-seq with DroNc-seq, Nat. Methods 14 (10) (2017) 955–958.
[18] Y. Hao, S. Hao, E. Andersen-Nissen, W.M. Mauck 3rd, S. Zheng, A. Butler, M.J. Lee, A.J. Wilk, C. Darby, M. Zager, et al., Integrated analysis of multimodal single-cell data, Cell 184 (13) (2021) 3573–3587.e3529.
[19] R. Xue, Q. Zhang, Q. Cao, R. Kong, X. Xiang, H. Liu, M. Feng, F. Wang, J. Cheng, Z. Li, et al., Liver tumour immune microenvironment subtypes and neutrophil heterogeneity, Nature 612 (7938) (2022) 141–147.
[20] M. Chaffin, I. Papangeli, B. Simonson, A.D. Akkad, M.C. Hill, A. Arduini, S.J. Fleming, M. Melanson, S. Hayat, M. Kost-Alimova, et al., Single-nucleus profiling of human dilated and hypertrophic cardiomyopathy, Nature 608 (7921) (2022) 174–180.
[21] G. Yu, L.G. Wang, Y. Han, Q.Y. He, clusterProfiler: an R package for comparing biological themes among gene clusters, OMICS A J. Integr. Biol. 16 (5) (2012) 284–287.
[22] K. Ishibashi, K. Ikegami, T. Shimbo, E. Sasaki, T. Kitayama, Y. Nakamura, T. Tsushima, Y. Ishibashi, K. Tamai, Single-cell transcriptome analysis reveals cellular heterogeneity in mouse intra- and extra articular ligaments, Commun. Biol. 5 (1) (2022) 1233.
[23] A.P. Skirving, T.J. Sims, A.J. Bailey, Congenital dislocation of the hip: a possible inborn error of collagen metabolism, J. Inherit. Metab. Dis. 7 (1) (1984) 27–31.
[24] H. Oda, M. Igarashi, Y. Hayashi, S. Karube, S. Inoue, R. Sakaguchi, M. Kimizuka, Soft tissue collagen in congenital dislocation of the hip. Biochemical studies of the ligamentum teres of the femur and the hip joint capsule, Nihon Seikeigeka Gakkai zasshi 58 (3) (1984) 331–338.
[25] Y. Wu, S. Yang, J. Ma, Z. Chen, G. Song, D. Rao, Y. Cheng, S. Huang, Y. Liu, S. Jiang, et al., Spatiotemporal immune landscape of Colorectal cancer liver Metastasis at single-cell level, Cancer Discov. 12 (1) (2022) 134–153.
[26] A. Liberzon, A. Subramanian, R. Pinchback, H. Thorvaldsdóttir, P. Tamayo, J.P. Mesirov, Molecular signatures database (MSigDB) 3.0, Bioinformatics 27 (12) (2011) 1739–1740.
[27] A. Liberzon, C. Birger, H. Thorvaldsdóttir, M. Ghandi, J.P. Mesirov, P. Tamayo, The Molecular Signatures Database (MSigDB) hallmark gene set collection, Cell systems 1 (6) (2015) 417–425.
[28] S. Aibar, C.B. González-Blas, T. Moerman, V.A. Huynh-Thu, H. Imrichova, G. Hulselmans, F. Rambow, J.C. Marine, P. Geurts, J. Aerts, et al., SCENIC: single-cell regulatory network inference and clustering, Nat. Methods 14 (11) (2017) 1083–1086.
[29] M. Andreatta, S.J. Carmona, UCell: robust and scalable single-cell gene signature scoring, Comput. Struct. Biotechnol. J. 19 (2021) 3796–3798.
[30] M. Foroutan, D.D. Bhuva, R. Lyu, K. Horan, J. Cursons, M.J. Davis, Single sample scoring of molecular phenotypes, BMC Bioinf. 19 (1) (2018) 404.

[31] S. Hänzelmann, R. Castelo, J. Guinney, GSVA: gene set variation analysis for microarray and RNA-seq data, BMC Bioinf. 14 (2013) 7.
[32] R. Kolde, S. Laur, P. Adler, J. Vilo, Robust rank aggregation for gene list integration and meta-analysis, Bioinformatics 28 (4) (2012) 573–580.
[33] W. Yan, Z. Hao, S. Tang, J. Dai, L. Zheng, P. Yu, W. Yan, X. Han, X. Xu, D. Shi, et al., A genome-wide association study identifies new genes associated with developmental dysplasia of the hip, Clin. Genet. 95 (3) (2019) 345–355.
[34] M. Dembic, L. van Brakel Andersen, M.J. Larsen, I. Mechlenburg, K. Søballe, J.M. Hertz, Whole exome sequencing of 28 families of Danish descent reveals novel candidate genes and pathways in developmental dysplasia of the hip, Mol. Genet. Genom. : MGG 298 (2) (2023) 329–342.
[35] M. Ginja, A.R. Gaspar, C. Ginja, Emerging insights into the genetic basis of canine hip dysplasia, Vet. Med. 6 (2015) 193–202.
[36] E. Kenanidis, N.K. Gkekas, A. Karasmani, P. Anagnostis, P. Christofilopoulos, E. Tsiridis, Genetic Predisposition to developmental dysplasia of the hip, J. Arthroplasty 35 (1) (2020) 291–300.e291.
[37] M.L. Doolittle, S. Khosla, D. Saul, Single-cell integration of BMD GWAS results Prioritize candidate genes influencing Age-related bone Loss, JBMR plus 7 (10) (2023) e10795.
[38] X. Qiu, H.Y. Wang, Z.Y. Yang, L.M. Sun, S.N. Liu, C.Q. Fan, F. Zhu, Uncovering the prominent role of satellite cells in paravertebral muscle development and aging by single-nucleus RNA sequencing, Genes & diseases 10 (6) (2023) 2597–2613.
[39] T. Rolland, M. Taşan, B. Charloteaux, S.J. Pevzner, Q. Zhong, N. Sahni, S. Yi, I. Lemmens, C. Fontanillo, R. Mosca, et al., A proteome-scale map of the human interactome network, Cell 159 (5) (2014) 1212–1226.
[40] D. Szklarczyk, A.L. Gable, K.C. Nastou, D. Lyon, R. Kirsch, S. Pyysalo, N.T. Doncheva, M. Legeay, T. Fang, P. Bork, et al., The STRING database in 2021: customizable protein-protein networks, and functional characterization of user-uploaded gene/measurement sets, Nucleic acids research 49 (D1) (2021) D605–d612.
[41] C. Fan, M. Liao, L. Xie, L. Huang, S. Lv, S. Cai, X. Su, Y. Wang, H. Wang, M. Wang, et al., Single-cell transcriptome integration analysis reveals the correlation between mesenchymal stromal cells and fibroblasts, Front. Genet. 13 (2022) 798331.
[42] G.S. Gulati, S.S. Sikandar, D.J. Wesche, A. Manjunath, A. Bharadwaj, M.J. Berger, F. Ilagan, A.H. Kuo, R.W. Hsieh, S. Cai, et al., Single-cell transcriptional diversity is a hallmark of developmental potential, Science (New York, NY) 367 (6476) (2020) 405–411.
[43] X. Qiu, A. Hill, J. Packer, D. Lin, Y.A. Ma, C. Trapnell, Single-cell mRNA quantification and differential analysis with Census, Nat. Methods 14 (3) (2017) 309–315.
[44] S. Jin, C.F. Guerrero-Juarez, L. Zhang, I. Chang, R. Ramos, C.H. Kuan, P. Myung, M.V. Plikus, Q. Nie, Inference and analysis of cell-cell communication using CellChat, Nat. Commun. 12 (1) (2021) 1088.
[45] X. Wu, W. Xu, L. Deng, Y. Li, Z. Wang, L. Sun, A. Gao, H. Wang, X. Yang, C. Wu, et al., Development of Multiomics in Situ Pairwise Sequencing (MiP-Seq) for Single-Cell Resolution Multidimensional Spatial Omics, 2023 523058, 2023.2001.2007.
[46] X. Qiu, H.-Y. Wang, Z.-Y. Yang, L.-M. Sun, S.-N. Liu, C.-Q. Fan, F.J.G. Zhu, Diseases, Uncovering the Prominent Role of Satellite Cells in Paravertebral Muscle Development and Aging by Single-Nucleus RNA Sequencing, 2023.
[47] Y. Chen, X. Zhang, X. Peng, Y. Jin, P. Ding, J. Xiao, C. Li, F. Wang, A. Chang, Q. Yue, et al., SPEED: single-cell Pan-species atlas in the light of Ecology and Evolution for development and diseases, Nucleic acids research 51 (D1) (2023) D1150–d1159.
[48] J.F. Ouyang, U.S. Kamaraj, E.Y. Cao, O.J.L. Rackham, ShinyCell: simple and sharable visualization of single-cell gene expression data, Bioinformatics 37 (19) (2021) 3374–3376.
[49] C. Yuan, Z. Pan, K. Zhao, J. Li, Z. Sheng, X. Yao, H. Liu, X. Zhang, Y. Yang, D. Yu, et al., Classification of four distinct osteoarthritis subtypes with a knee joint tissue transcriptome atlas, Bone research 8 (1) (2020) 38.
[50] A.J. De Micheli, J.B. Swanson, N.P. Disser, L.M. Martinez, N.R. Walker, D.J. Oliver, B.D. Cosgrove, C.L. Mendias, Single-cell transcriptomic analysis identifies extensive heterogeneity in the cellular composition of mouse Achilles tendons, American journal of physiology Cell physiology 319 (5) (2020) C885–c894.
[51] Q. Li, R. Xu, K. Lei, Q. Yuan, Insights into skeletal stem cells, Bone research 10 (1) (2022) 61.
[52] J. He, J. Yan, J. Wang, L. Zhao, Q. Xin, Y. Zeng, Y. Sun, H. Zhang, Z. Bai, Z. Li, et al., Dissecting human embryonic skeletal stem cell ontogeny by single-cell transcriptomic and functional analyses, Cell Res. 31 (7) (2021) 742–757.
[53] K. Wilk, S.A. Yeh, L.J. Mortensen, S. Ghaffarigarakani, C.M. Lombardo, S.H. Bassir, Z.A. Aldawood, C.P. Lin, G. Intini, Postnatal Calvarial skeletal stem cells expressing PRX1 Reside exclusively in the Calvarial sutures and are required for bone regeneration, Stem Cell Rep. 8 (4) (2017) 933–946.
[54] R.Y. Ma, A. Black, B.Z. Qian, Macrophage diversity in cancer revisited in the era of single-cell omics, Trends Immunol. 43 (7) (2022) 546–563.
[55] L. Muhl, G. Genové, S. Leptidis, J. Liu, L. He, G. Mocci, Y. Sun, S. Gustafsson, B. Buyandelger, I.V. Chivukula, et al., Single-cell analysis uncovers fibroblast heterogeneity and criteria for fibroblast and mural cell identification and discrimination, Nat. Commun. 11 (1) (2020) 3953.
[56] X.B. Zhao, Y.P. Chen, M. Tan, L. Zhao, Y.Y. Zhai, Y.L. Sun, Y. Gong, X.Q. Feng, J. Du, Y.B. Fan, Extracellular matrix stiffness regulates DNA Methylation by PKCα-Dependent nuclear Transport of DNMT3L, Adv. Healthcare Mater. 10 (16) (2021) e2100821.
[57] C. Kuppe, M.M. Ibrahim, J. Kranz, X. Zhang, S. Ziegler, J. Perales-Patón, J. Jansen, K.C. Reimer, J.R. Smith, R. Dobie, et al., Decoding myofibroblast origins in human kidney fibrosis, Nature 589 (7841) (2021) 281–286.
[58] C. Li, Z. Peng, Y. Zhou, Y. Su, P. Bu, X. Meng, B. Li, Y. Xu, Comprehensive analysis of pathological changes in hip joint capsule of patients with developmental dysplasia of the hip, Bone & joint research 10 (9) (2021) 558–570.
[59] L. Cerezal, J. Arnaiz, A. Canga, T. Piedra, J.R. Altónaga, R. Munafo, L. Pérez-Carro, Emerging topics on the hip: ligamentum teres and hip microinstability, European journal of radiology 81 (12) (2012) 3745–3754.
[60] U. Proske, S.C. Gandevia, The proprioceptive senses: their roles in signaling body shape, body position and movement, and muscle force, Physiol. Rev. 92 (4) (2012) 1651–1697.
[61] K.K.L. Lau, K.K.P. Law, K.Y.H. Kwan, J.P.Y. Cheung, K.M.C. Cheung, A.Y.L. Wong, Timely Revisit of proprioceptive deficits in adolescent idiopathic scoliosis: a Systematic review and meta-analysis, Global Spine J. 12 (8) (2022) 1852–1861.
[62] A.T. Chesler, M. Szczot, D. Bharucha-Goebel, M. Čeko, S. Donkervoort, C. Laubacher, L.H. Hayes, K. Alter, C. Zampieri, C. Stanley, et al., The role of PIEZO2 in human Mechanosensation, N. Engl. J. Med. 375 (14) (2016) 1355–1364.
[63] M.V. Plikus, X. Wang, S. Sinha, E. Forte, S.M. Thompson, E.L. Herzog, R.R. Driskell, N. Rosenthal, J. Biernaskie, V. Horsley, Fibroblasts: origins, definitions, and functions in health and disease, Cell 184 (15) (2021) 3852–3872.
[64] J.F. Martin, A. Bradley, E.N. Olson, The paired-like homeo box gene MHox is required for early events of skeletogenesis in multiple lineages, Genes & development 9 (10) (1995) 1237–1249.
[65] T. Qin, G. Zhang, Y. Zheng, S. Li, Y. Yuan, Q. Li, M. Hu, H. Si, G. Wei, X. Gao, et al., A population of stem cells with strong regenerative potential discovered in deer antlers, Science (New York, NY) 379 (6634) (2023) 840–847.
[66] R. Wynne-Davies, Acetabular dysplasia and familial joint laxity: two etiological factors in congenital dislocation of the hip. A review of 589 patients and their families, The Journal of bone and joint surgery British 52 (4) (1970) 704–716.
[67] S. Zhang, J. Song, Q. Wu, J. Fang, B. Ning, Collagen I in the hip capsule plays a role in Postoperative Clinical function in patients with developmental dysplasia of the hip, Frontiers in pediatrics 10 (2022) 918660.
[68] L. Zhao, W. Tian, H. Pan, X. Zhu, J. Wang, Z. Cheng, L. Cheng, X. Ma, B. Wang, Variations of the COL1A1 gene promoter and the relation to developmental dysplasia of the hip, Genet. Test. Mol. Biomarkers 17 (11) (2013) 840–843.
[69] A.R. Aricescu, C. Siebold, K. Choudhuri, V.T. Chang, W. Lu, S.J. Davis, P.A. van der Merwe, E.Y. Jones, Structure of a tyrosine phosphatase adhesive interaction reveals a spacer-clamp mechanism, Science (New York, NY) 317 (5842) (2007) 1217–1220.
[70] G.C. Zondag, A.B. Reynolds, W.H. Moolenaar, Receptor protein-tyrosine phosphatase RPTPmu binds to and dephosphorylates the catenin p120(ctn), J. Biol. Chem. 275 (15) (2000) 11264–11269.
[71] X. Tang, Y. Miao, Y. Luo, K. Sriram, Z. Qi, F.M. Lin, Y. Gu, C.H. Lai, C.Y. Hsu, K.L. Peterson, et al., Suppression of endothelial AGO1 promotes adipose tissue Browning and Improves metabolic dysfunction, Circulation 142 (4) (2020) 365–379.

[72] C. Crewe, N. Joffin, J.M. Rutkowski, M. Kim, F. Zhang, D.A. Towler, R. Gordillo, P.E. Scherer, An endothelial-to-adipocyte extracellular vesicle Axis governed by metabolic state, Cell 175 (3) (2018) 695–708.e613.
[73] Y. Chen, H. Wang, Q. Yang, W. Zhao, Y. Chen, Q. Ni, W. Li, J. Shi, W. Zhang, L. Li, et al., Single-cell RNA landscape of the osteoimmunology microenvironment in periodontitis, Theranostics 12 (3) (2022) 1074–1096.
[74] X. Huang, N. Yang, V.F. Fiore, T.H. Barker, Y. Sun, S.W. Morris, Q. Ding, V.J. Thannickal, Y. Zhou, Matrix stiffness-induced myofibroblast differentiation is mediated by intrinsic mechanotransduction, American journal of respiratory cell and molecular biology 47 (3) (2012) 340–348.
[75] E. Trimm, Red-Horse K: **vascular endothelial cell development and diversity**, Nat. Rev. Cardiol. 20 (3) (2023) 197–210.
[76] V. Perumal, S.J. Woodley, H.D. Nicholson, Neurovascular structures of the ligament of the head of femur, J. Anat. 234 (6) (2019) 778–786.
[77] H. Wang, X. Zhang, J.Y. He, X.F. Zheng, D. Li, Z. Li, J.F. Zhu, C. Shen, G.Q. Cai, X.D. Chen, Increasing expression of substance P and calcitonin gene-related peptide in synovial tissue and fluid contribute to the progress of arthritis in developmental dysplasia of the hip, Arthritis Res. Ther. 17 (1) (2015) 4.
[78] M.L. Doolittle, G.M. Calabrese, L.D. Mesner, D.A. Godfrey, R.D. Maynard, C.L. Ackert-Bicknell, C.R. Farber, Genetic analysis of osteoblast activity identifies Zbtb40 as a regulator of osteoblast activity and bone mass, PLoS Genet. 16 (6) (2020) e1008805.